BOLETIN DE LA SOCIEDAD ESPAÑOLA DE
Cerámica y Vidrio
www.elsevier.es/bsecv

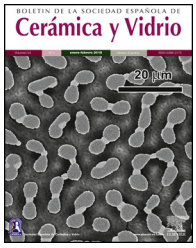

Neutron diffraction residual stress analysis of Al_2O_3/Y-TZP ceramic composites

Kunyang Fan[a], *Jesús Ruiz-Hervias*[a,*], *Jonas Gurauskis*[b], *Antonio J. Sanchez-Herencia*[b], *Carmen Baudín*[b]

[a] *Materials Science Department, Universidad Politécnica de Madrid, E.T.S.I. Caminos, Canales y Puertos, C/Profesor Aranguren s/n, E-28040 Madrid, Spain*
[b] *Instituto de Cerámica y Vidrio, CSIC, Kelsen 5, E-28049 Madrid, Spain*

ARTICLE INFO

Article history:
Received 13 October 2015
Accepted 27 October 2015
Available online 20 November 2015

Keywords:
Ceramics
Residual stresses
Neutron diffraction
Tape casting

ABSTRACT

Residual stress measurements were conducted by time-of-flight neutron diffraction and Rietveld analysis method in Al_2O_3/Y-TZP ceramic composites fabricated by different green processing techniques (a novel tape casting and conventional slip casting) and with different Y-TZP content (5 and 40 vol.% Y-TZP). The results show that the residual stresses in Y-TZP particulates are tensile and the ones in Al_2O_3 matrix are compressive, with almost flat through-thickness residual stress profiles in all bulk samples. As Y-TZP content increased, tension in Y-TZP phase was decreased but compression in Al_2O_3 matrix was increased (in absolute value). The values of residual stresses for both phases were mainly dependent on the Y-TZP content in the studied Al_2O_3/Y-TZP composites, irrespective of sample orientation and fabrication processes (a novel tape casting and conventional slip casting).

Análisis de tensiones residuales por difracción de neutrones en materiales compuestos cerámicos de Al_2O_3/Y-TZP

Palabras clave:
Cerámicos
Tensiones residuales
Difracción de neutrones
Colaje en cinta

RESUMEN

Se han hecho medidas de tensiones residuales por difracción de neutrones mediante la técnica de tiempo de vuelo en muestras de compuestos cerámicos de Al_2O_3/Y-TZP (alumina-circonia) fabricados por dos técnicas diferentes de procesado en verde (colaje en cinta y colaje convencional) y con distinto contenido de Y-TZP (5% y 40% en volumen, respectivamente). Los resultados se han analizado usando el método de Rietveld y muestran que las tensiones residuales en las partículas de Y-TZP son de tracción mientras que en la matriz de alúmina son de compresión, con perfiles de tensiones residuales casi planos a lo largo del espesor de las muestras. A medida que aumenta el contenido de Y-TZP, las tensiones residuales de tracción en esa fase disminuyen, mientras que las tensiones de compresión

* *Corresponding author.*
E-mail address: jesus.ruiz@upm.es (J. Ruiz-Hervias).
http://dx.doi.org/10.1016/j.bsecv.2015.10.006

en la matriz de alumina aumentan (en valor absoluto). Se ha demostrado que los valores de las tensiones residuales en ambas fases dependen fundamentalmente del contenido de zirconia en los compuestos estudiados, independiente de la dirección de medida y el proceso de fabricación (colaje en cinta frente a colaje convencional).

Introduction

Alumina–zirconia composites are extensively used in different applications, such as insulators, refractory uses, cutting tools, high temperature filtering and biomedical application [1,2], due to the improved mechanical behavior when compared with that of monophase alumina [3–6]. Many research papers have been devoted to study the toughening mechanisms of alumina–zirconia composites [7–10]. Besides the well-known stress-induced transformation toughening and microcracking toughening [7,10–13], it has been proposed that the residual stresses due to thermal and elastic mismatches between alumina and zirconia could also contribute to toughening and enhance the structural performance of these ceramic composites [14–16]. It was anticipated that the maximum levels of beneficial residual stress could be raised by approximately one order of magnitude, leading to a wide variety of possible toughening mechanisms: crack deflection, crack branching, crack bridging and microcracking [13,17,18]. Furthermore, the development of internal residual stresses, in addition to externally applied ones, may induce a martensitic transformation (tetragonal to monoclinic) in zirconia [14], which would significantly affect mechanical performance.

The recent development of laminated ceramic structures requires understanding of the nature of the residual stresses in order to obtain defect-free structures with operative reinforcing layers. Besides the effect of laminate designs (layer structure and thickness) on macroscopic stress field between adjacent layers [19–22], the detailed micro-residual stresses information in each layer is very important to clarify the reinforcing mechanisms as well as to optimize the resulting residual stress field, with the aim of improving the mechanical properties of ceramics. Micromechanical analyses predicted that internal residual stresses of ceramics could be varied by an appropriate selection of the fabrication process and materials design [2,23]. The effects associated to composition should be separated to those related to the laminate stacking design, in order to have a better control over the manufacturing process.

Several research works have been done on the residual stress (RS) analysis of Al_2O_3-ZrO_2 composites (see for instance references [16,19,24–27]). In those works, different measurement techniques were used, namely Raman spectroscopy, X-ray and neutron diffraction, in materials with different fabrication routes and composition.

Previous studies [27,28] have successfully assessed the presence of residual stresses in alumina–zirconia composite ceramics by constant-wavelength neutron diffraction measurement. The obtained information was limited from single diffraction peak measurements in each phase. Due to the thermal and elastic crystal anisotropy and the complexity of microstructure, residual strains from single peak diffraction measurements might not represent the bulk material behavior [29]. In order to access more detailed information on residual stresses, both in the micro-scale and in the bulk, as well as to monitor the phase composition in sintered ceramics, time-of-flight (TOF) neutron diffraction (ND) technique is particularly useful. It is a superior way of internal strain measurement with high resolution, high penetration of neutrons into matter and high-efficiency for collecting large quantities of data over numerous diffraction peaks simultaneously from the whole diffraction pattern [30]. This way through-thickness stress profiles can be obtained in the bulk, which are not affected by surface effects. By combining TOF measurements with the well-known whole profile structure refinement method—Rietveld refinement [31], a wealth of information ranging from the crystal structure and phase analysis, to the residual stresses can be obtained.

The conventional slip casting technique [32] has been accepted as a simple, reliable and economical process technology for many years. New tape casting routes were used to produce alumina–zirconia composites [33,34], which involved the stacking of green ceramics tapes at room temperature and using low pressures. The use of low content of organic additions was better both from the economic and environmental point of view. In addition, this process resulted in the optimum properties, by minimizing interface defects, anisotropy, high porosity and even cracking that existed in traditional tape casting, for producing laminated materials. In order to take full advantage of the novel tape casting method into the production of alumina–zirconia laminated materials, it is meaningful to investigate the residual stresses by comparison to the materials produced by slip casting. Moreover, the addition of zirconia was reported to significantly influence on the microstructure and mechanical properties of materials [35]. In order to meet the requirement of co-sintering of layers with different composition in laminated materials, effect of addition of zirconia on residual stress development of alumina–zirconia ceramics were taken into investigations. The phase compositions in sintered ceramics especially the ones of zirconia should be accurately examined, due to the complex polymorph of ZrO_2 [40] and the possible phase transformation during fabrication process.

In this paper, time-of-flight neutron diffraction and Rietveld analysis was applied to precisely determine the residual stress profiles in alumina reinforced with 3 mol.% yttria-stabilized zirconia composites (Al_2O_3/Y-TZP). Different zirconia contents and green processing routes were investigated (the novel tape casting and conventional slip casting). Through-thickness residual stress profiles of the alumina matrix and the zirconia particulates were obtained for all

studied Al_2O_3/Y-TZP composites, and compared to available data in the literature and to estimations by theoretical models. The effects of the addition of second phase zirconia and green processing were related to the residual stress field and the observed microstructure.

Experimental

Sample preparation

The materials to be studied were prepared using high-purity α-Al_2O_3 (Condea HPA 0.5, USA, d_{50} = 0.35 μm and S_s = 9.5 m^2/g) and polycrystalline tetragonal zirconia stabilized with 3 mol. % Y_2O_3 (TZ3YS, TOSOH, Japan, d_{50} = 0.4 μm and S_s = 6.7 m^2/g), named as Y-TZP, as the starting powders. Two compositions, 95 vol.% of α-Al_2O_3 with 5 vol.% of Y-TZP (named A-5YTZP) and 60 vol.% of α-Al_2O_3 with 40 vol.% of Y-TZP (named A-40YTZP), were selected. Two kinds of green processing methods were used in fabrication for each composition: the novel tape casting [33,34], and conventional slip casting, as a reference route. The studied specimens were named as A-5YTZP(slip), A-5YTZP(tape), A-40YTZP(slip) and A-40YTZP(tape), in order to describe compositions and fabrication techniques.

Stable slurries were prepared by mixing the starting powders with 47 vol.% of solid content in deionized water, using a polyelectrolyte (Dolapix CE 64, Zschimmer and Schwarz, Germany) as dispersant. Slurries were ball milled for 4 h using alumina jar and balls. One series was fabricated by slip casting of the deflocculated suspensions in plaster mold and leaving them to dry for 24 h. The other series was fabricated by tape casting on a polypropylene film using a moving tape-casting device with two doctor blades using a 10 mm/s casting velocity and a 500 μm gap height between the blades and the carrier film. After tape casting, the green ceramic tapes were dried at room temperature for 24 h and subsequently at 60 °C degrees for 48 h. A water-based polymeric emulsion Mowilith DM 765 E (Celanese, Tarragona, Spain), with solid content 50 vol.%, particle size 0.05–0.15 mm, was used as the binder emulsion. The final thickness of the green tapes varied between ~480 μm and 520 μm. Monolithic piece was prepared by stacking 11 layers of the same compositions tapes together and applying a gluing agent (5 wt.% dilution in distilled water of the binder) under uniaxial pressure of 18 MPa at room temperature. A detailed description of the green processing and pressing procedure are given elsewhere [33,34].

All the green samples were machined into bars (approximately 40 mm × 40 mm × 5 mm) and the surfaces were smoothed with sandpaper. For binder burnout, green bodies were pre-sintered at 600 °C for 30 min, with a heating rate of 1 °C/min. Subsequent sintering was carried out at maximum temperature of 1500 °C, with a dwell of 2 h (heating and cooling rates of 5 °C/min).

Characterization

The density of the sintered samples, measured by Archimedes's method (European Standard EN 1389:2003), is reported in Table 1 (average values of five measurements, and standard deviation as error). Relative densities were calculated as a percentage of the calculated theoretical density for each composition, using 3.99 g/cm^3 for α-Al_2O_3 (ASTM 42-1468) and 6.10 g/cm^3 for Y-TZP (ASTM 83-113). Microstructural characterization was performed by scanning electron microscopy (SEM, Zeiss DSM 950, Germany) on diamond polished (down to 1 μm) and chemically etched (85% H_3PO_4, 7 min at 200 °C) surfaces. The average grain sizes of Al_2O_3 and Y-TZP particles were determined by the linear intercept method considering at least 200 grains for each phase. The A/Y-TZP samples information with density and average grain size were reported in Table 1. High densities (relative density > 98%) were found in all the studied A/Y-TZP composites. As the zirconia content increased, the density was also increased and the grain size of Al_2O_3 matrix was decreased, due to the constriction imposed by the second phase zirconia particles on matrix grain growth. The results seem not to depend on the particular casting technique, which indicates that the microstructure quality was assured in ceramics fabricated by the novel tape casting method, with defect-free interfaces between individual tapes.

Residual stresses measurement

For neutron diffraction strain scanning, samples in the shape of parallelepipeds with dimensions 20 mm × 20 mm × 5 mm were employed. In the pieces fabricated from tape casting, the larger surfaces (20 × 20 mm^2) were parallel to the surface of the stacked tapes.

Residual strain measurements were performed by neutron diffraction on ENGIN-X time-of-flight (TOF) instrument, a third-generation neutron strain scanner, operating at the ISIS spallation neutron source in the Rutherford Laboratory, UK. Details of this instrument are given in [35]. The experimental setup consists of two detector banks which are centered on Bragg angles of $2\theta_B = \pm 90$ degrees, as shown in Fig. 1. It allows

Table 1 – Values of measured density (ρ), relative density ($\rho_{relative}$) and average grain size (G) in A/Y-TZP composites investigated.

	Y-TZP (vol.%)	Casting techniques	ρ (g/cm^3)	$\rho_{relative}$ (T.D. %)	G (μm)	
					G_A	$G_{Y\text{-}TZP}$
A-5YTZP(slip)	5	Slip casting	4.03 ± 0.06	98.4 ± 0.1	1.9 ± 0.3	0.3 ± 0.1
A-5YTZP(tape)	5	Tape casting	4.02 ± 0.06	98.2 ± 0.2		
A-40YTZP(slip)	40	Slip casting	4.77 ± 0.07	98.7 ± 0.2	1.0 ± 0.2	0.5 ± 0.2
A-40YTZP(tape)	40	Tape casting	4.76 ± 0.02	98.5 ± 0.1		

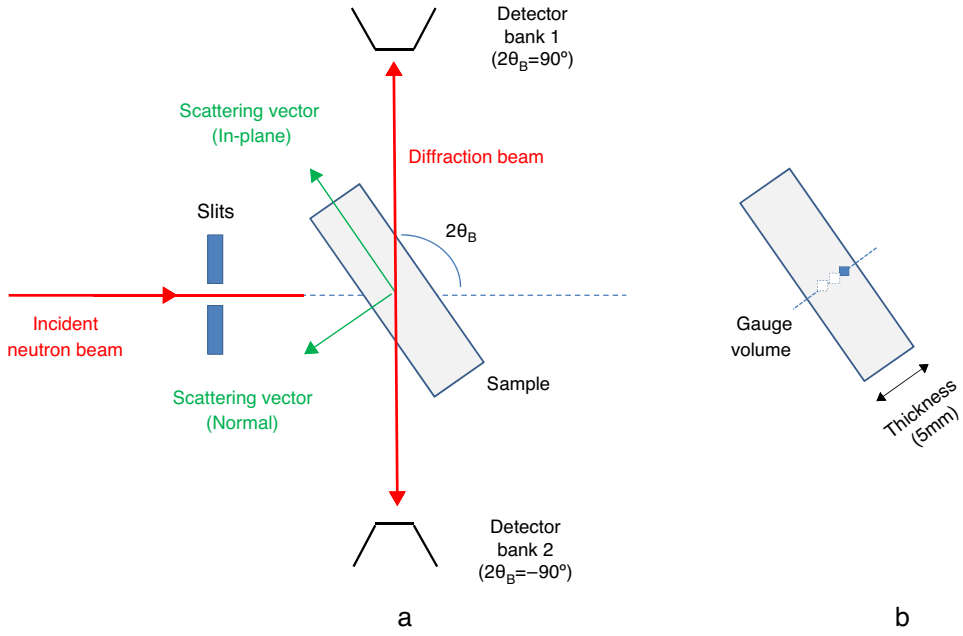

Fig. 1 – Experimental set-up on the time-of-flight neutron strain scanner ENGIN-X at ISIS. (a) Residual strains were collected both in the in-plane and normal direction. (b) Strain scanning was carried out along the sample thickness with the interior gauge volume.

simultaneous measurements of strain in two directions: the in-plane direction, parallel to the larger plane of the samples (20 mm × 20 mm), and the normal direction, perpendicular to it, which are assumed to be the principal stress component directions. The fabrication process is assumed to produce a transversely isotropic stress state, where the stresses in the larger plane of the sample are equal. Consequently, only the in-plane and the normal directions are needed for residual stress determination.

The measurement gauge volume was set to $15 \times 1 \times 1\,mm^3$, defined by incident horizontal and vertical cadmium slits and a radial collimator slit in front of each detector bank. The centroid of this gauge volume defines the location of the measurement. Strain scanning was carried out along sample thickness (thickness of 5 mm), with measurement point interval of 0.4 mm.

The stress-free reference lattice parameters of α-Al_2O_3 and Y-TZP were obtained by measuring both of the α-Al_2O_3 and Y-TZP original powders. In this case, the gauge volume was set to $16 \times 3 \times 1\,mm^3$ in order to improve the counting statistics. This way the stress-free reference lattice parameters could be accurately determined. In addition, CeO_2 powder, used on the ENGIN-X instrument as an experimental standard, was measured to calibrate the peak profile parameters. All measurements were carried out at room temperature.

Data analysis

In TOF diffraction measurements, the whole diffraction patterns were obtained from each measurement point in bulk samples. The program TOPAS-Academic V5 [36] was employed to analyze the diffraction patterns by Rietveld refinement.

Rietveld refinement

As a well-known whole profile structure refinement method, Rietveld refinement is powerful for determining complete crystal structures (e.g. lattice parameters, atomic coordinates, occupancy, etc.), microstructure information and the residual stresses in a multiphase material. Quantitative phase analysis can be done by Rietveld analysis in TOPAS software.

The ENGIN-X instrument diffraction profile was modeled using a convolution of a pseudo-Voigt function $pV(t)$ (a linear combination of a Lorentzian function and Gaussian function) with two back-to-back exponentials $E(t)$ [37]. Data of CeO_2 standard powder (cubic phase, space group $Fm\bar{3}m$, $a = 5.4114$ Å) was refined to calibrate instrument-dependent diffractometer constants and profile parameters. The obtained parameters were then fixed and used for refinements of bulk samples and stress-free references powders, according to their corresponding gauge volume setting.

In consideration of the complex polymorph of ZrO_2 [38], especially the possible tetragonal to monoclinic transformation during fabrication process, Rietveld refinement trials have been done for zirconia starting powder and A/Y-TZP bulk samples, with crystal structures of tetragonal (*t*) Y_2O_3-doped ZrO_2 (Y-TZP) [39], monoclinic (*m*) ZrO_2 [38] and cubic (*c*) Y_2O_3-doped ZrO_2 [38] being introduced simultaneously. The fitting results confirmed no existence of cubic zirconia phase in both Y-TZP starting powder and A/Y-TZP composites. Around 70 vol.% tetragonal Y-TZP and 30 vol.% monoclinic phase were detected in zirconia starting powder, as shown in the diffraction profile of Fig. 2. However, in A/Y-TZP composites, only phases of α-Al_2O_3 matrix and tetragonal Y-TZP were detected, without monoclinic zirconia. Therefore, in this work, the Rietveld

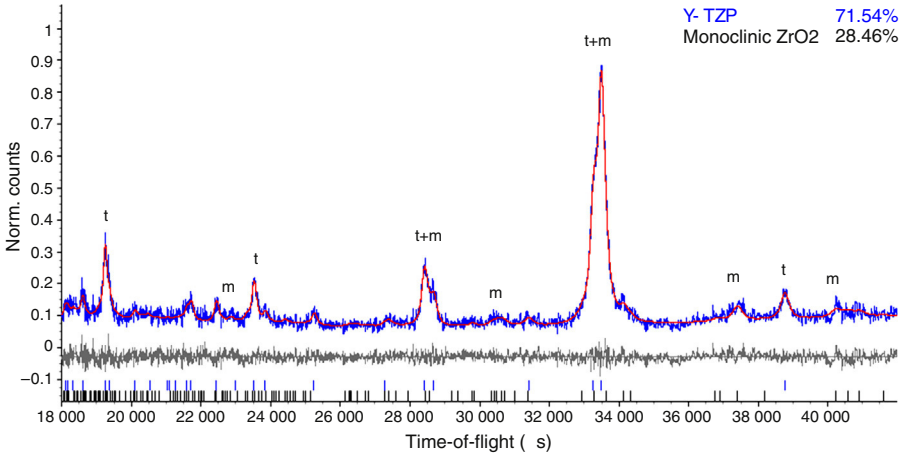

Fig. 2 – Time-of-flight neutron diffraction patterns analyzed with Rietveld refinement for Y-TZP starting powders. Tetragonal Y-TZP (t) and monoclinic ZrO_2 (*m*) were detected in zirconia starting powder, with the corresponding diffraction peaks being identified at the bottom of profiles with blue tick marks and black ones, respectively.

refinements of zirconia starting powder were done with both *m*-ZrO_2 and tetragonal Y-TZP crystal structures. All A/Y-TZP composites were analyzed by using a two-phase model consisting of the hexagonal α-Al_2O_3 phase [40] and tetragonal Y-TZP phase [39].

Variable parameters like lattice parameters, atomic coordinates, isotropic thermal parameters, scale factors and polynomial background parameters, etc. were refined during the analysis. All the refinements were conducted step-by-step to avoid correlation effects between parameters [41]. The space groups and initial atomic structure information used in refinements are listed in Table 2. The overall quality of fitting was assessed in terms of *R* values [41], as obtained from the refinements.

Stress determination

With Rietveld refinement of the entire diffraction spectrum, lattice parameters of each phase in composites can be obtained. The mean phase strain, given by a weighted average of several single-peak strains, was determined from the change of average lattice parameters in Rietveld refinements of the entire diffraction spectrum [42]. Taking all diffraction peaks into account allows us to represent the bulk behavior more effectively, and to determine residual strain more reliably in ceramic composites.

In this study, for hexagonal α-Al_2O_3 phase, strain can be calculated along lattice axis:

$$\varepsilon_a = \frac{a - a_0}{a_0} \quad (1)$$

$$\varepsilon_c = \frac{c - c_0}{c_0} \quad (2)$$

where a ($a = b$) and c are the lattice parameters of α-Al_2O_3 phase, and a_0 and c_0 are the stress-free lattice parameters measured from Al_2O_3 starting powder. For the tetragonal Y-TZP, strain in a ($a = b$) and c axis can be determined in the same way.

Ignoring the local variations that occur around the particles, integration is performed over randomly oriented grains in composites. Without accounting for granular anisotropy, mean phase strains in the gauge volume were calculated by averaging the strain over the unit cell, for Al_2O_3 and Y-TZP phase [43]:

$$\bar{\varepsilon}_A = \frac{1}{3}(2\varepsilon_a + \varepsilon_c)_A \quad (3)$$

Table 2 – Initial crystal structure parameters used in refinement.

Phase	Space group	Lattice parameter/Å	Ionic position and coordinate			
			ion	x	y	z
α-Al_2O_3 [40] (hexagonal)	$R\bar{3}c$	$a = b = 4.7602$ $c = 12.9933$ $\alpha = \beta = 90°$ $\gamma = 120°$	Al^{3+} O^{2-}	0 0.30624	0 0	0.35216 0.25
Y-TZP [39] (tetragonal)	P42/nmc	$a = b = 3.6183$ $c = 5.1634$ $\alpha = \beta = \gamma = 90°$	Zr^{4+} Y^{3+} O^{2-}	0 0 0	0 0 0.5	0 0 0.217
m-ZrO_2 [38] (monoclinic)	P21/c	$a = 5.1505$ $b = 5.2116$ $c = 5.3173 \beta = 99.23°$	Zr^{4+} O_1^{2-} O_2^{2-}	0.2754 0.07 0.4496	0.0395 0.3317 0.7569	0.2083 0.3447 0.4792

$$\bar{\varepsilon}_{\text{Y-TZP}} = \frac{1}{3}(2\varepsilon_a + \varepsilon_c)_{\text{Y-TZP}} \quad (4)$$

As explained above, taking into account the fabrication process and specimen symmetry, strains in the larger plane of samples are considered isotropic. Thus, strain measured in one in-plane and normal directions are enough for stress determination, and they are employed as the principal strains ε_{ii}, i = 1, 2, 3, as $\varepsilon_{11} = \varepsilon_{22} = \varepsilon_{\text{In-plane}}$ and $\varepsilon_{33} = \varepsilon_{\text{Normal}}$. Thus, mean phase stresses for both alumina and zirconia phases were determined in directions of in-plane and normal using Hooke's law, respectively, as:

$$\sigma_{\text{In-plane}} = \frac{E}{1+\nu}\bar{\varepsilon}_{\text{In-plane}} + \frac{E\nu}{(1+\nu)(1-2\nu)}(2\bar{\varepsilon}_{\text{In-plane}} + \bar{\varepsilon}_{\text{Normal}}) \quad (5)$$

$$\sigma_{\text{Normal}} = \frac{E}{1+\nu}\bar{\varepsilon}_{\text{Normal}} + \frac{E\nu}{(1+\nu)(1-2\nu)}(2\bar{\varepsilon}_{\text{In-plane}} + \bar{\varepsilon}_{\text{Normal}}) \quad (6)$$

where $\bar{\varepsilon}$ corresponds to the calculated mean phase strain for both Al_2O_3 and Y-TZP phases, given by Eqs. (3) and (4), E and ν are the bulk elastic constants of Al_2O_3 (E = 400 GPa and $\nu = 0.22$) and Y-TZP (E = 210 GPa and $\nu = 0.31$) [44].

Results and discussion

Microstructure

Characteristic microstructures of the studied Al_2O_3/Y-TZP composites are shown in Fig. 3, as a function of zirconia content. Very similar microstructures were exhibited by slip casting and tape casting A/Y-TZP samples with the same composition, thus the representative scanning electron micrographs of A-5YTZP and A-40YTZP composites were presented in Fig. 3(a) and (b), respectively, on behave of both slip casting and tape casting samples. Dense microstructure was observed in all the studied materials, where the alumina matrix (in dark gray) and zirconia particulates (in light gray) were generally well-dispersed. The grain size of Al_2O_3 matrix was obviously decreased as zirconia content increased. Narrow grain size distributions were observed for both phases in each composite. In A-5YTZP composites (Fig. 3(a)), the fine zirconia particulates were homogeneously distributed and located mainly at the triple points and grain boundaries of alumina matrix. In A-40YTZP composites (Fig. 3(b)), with more addition of Y-TZP second phase, the interconnection between Y-TZP grains were apparently increased. Some of Y-TZP particles clustered together as submatrix, where alumina grains were separated and surrounded by Y-TZP particulates.

Neutron diffraction patterns and Rietveld analysis

Fig. 4 shows a representative diffraction pattern for A-40YTZP (tape) composites, including raw measurements (blue line) and associated calculated profile (red line, overlapping the blue observed profiles). Individual peaks of α-Al_2O_3 and Y-TZP phases were identified with blue and black tick marks at the bottom of the profiles, respectively. The difference plot between the observed and calculated intensities was shown in gray line, below spectrums. As observed in Fig. 4, an almost flat difference line was obtained, which indicates the quality of fit. Good fitting was achieved for all reference powders and bulk samples, with the weighed residual error R_{wp} ranging from 4% to 10%.

The Rietveld refinement of the two-phase model consisting of α-Al_2O_3 phase and tetragonal Y-TZP phase was highly satisfactory for all A/Y-TZP composites samples, without evidence of the m-ZrO_2 phase as can be seen in Fig. 4. This shows that almost all the monoclinic phase in the zirconia starting powder was transformed to tetragonal structure during heating at high temperature (around 1170 °C) [45]. No transformation from tetragonal zirconia to monoclinic zirconia ($t \rightarrow m$ transformation) occurred during cooling process from the high sintering temperature to room temperature, in agreement with published [25,46]. This could be explained by the stabilizing action of Y_2O_3 on zirconia, as well as the restraint from phase-change volume expansion by Al_2O_3 matrix during cooling. As a consequence, the existence of residual stresses between Al_2O_3 matrix and Y-TZP inclusion were anticipated.

Comparing the diffraction spectrums of A-5YTZP and A-40YTZP, peak intensities of Al_2O_3 matrix were reduced as the zirconia content was increased (with an increase of Y-TZP peak intensities). No obvious differences were observed between

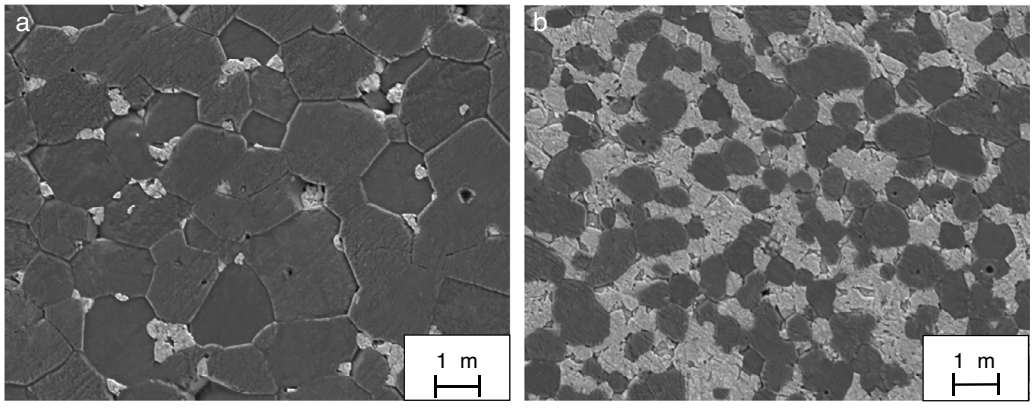

Fig. 3 – SEM micrographs of polished and chemical etched surfaces of the studied materials: (a) A-5YTZP composites, on behave of both slip casting and tape casting samples. (b) A-40YTZP composites, on behave of both slip casting and tape casting samples. Al_2O_3 grains appear with dark gray color and Y-TZP particulates are in (bright) light gray color.

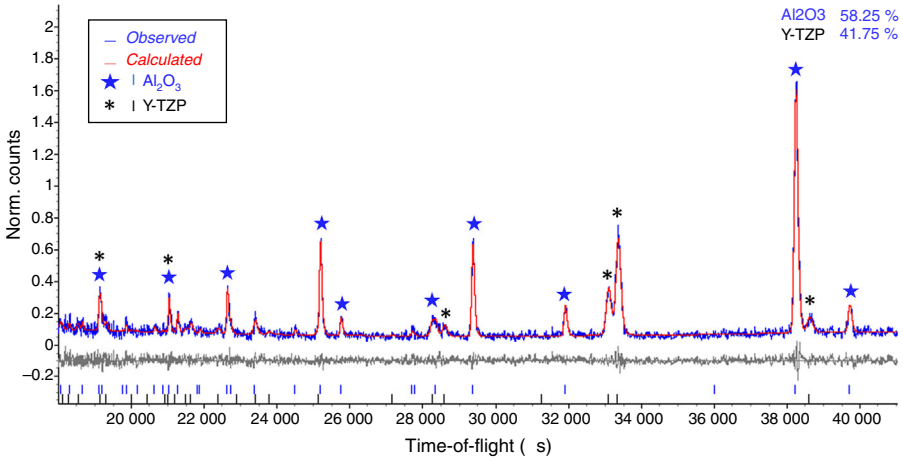

Fig. 4 – Representative TOF neutron diffraction patterns analyzed with Rietveld refinement for A-40YTZP(tape) samples. Individual peaks of Al_2O_3 (★) and Y-TZP (*) were identified at the bottom of profiles with blue tick marks and black ones, respectively.

spectra of slip casting samples and tape casting samples with the same Y-TZP vol.%. In addition, at the same scanning point, differences between spectra of in-plane and normal direction (measured at $2\theta = \pm 90^\circ$) are not significant, which indicates almost homogenous phase and microstructure distribution in materials.

Phase quantities corresponding to the measured gauge volumes were evaluated in Rietveld refinement, and the volume fraction is shown in the upper right of the profile fitting window (Fig. 4). Almost constant Y-TZP contents were detected in different scanning positions of the same sample, with 5 ± 2 vol.% in A-5YTZP composites and 40 ± 3 vol.% in A-40YTZP composites, which were very close to the nominal values.

Residual stress determination

In TOF measurement, mean phase stresses, as the averaged stresses for each phase over a large number of randomly oriented grains within the gauge volume area, were calculated by using the change of average lattice parameters for Al_2O_3 and Y-TZP phases, as shown by Eqs. (1)–(6). The through-thickness mean phase stresses profiles along the in-plane and normal directions were depicted for both the conventional slip casting (Fig. 5) and the novel tape casting routes (Fig. 6). In this case the error bars of mean phase stresses related to statistical uncertainties of the determined lattice parameters are smaller than the size of the symbols employed in the graphs.

As expected [24,25], the residual stresses were compressive in Al_2O_3 matrix and tensile in the Y-TZP particles, due to the lower thermal expansion coefficient of Al_2O_3 matrix as compared with Y-TZP particles. Quite homogeneous stress profiles through sample thickness were found for both phases in each specimen, as can be seen in Figs. 5 and 6, especially in the Al_2O_3 matrix, which agrees with a homogenous distribution of residual stress inside the samples. For the sample fabricated by tape casting, each measurement point always encompasses at least three individual tapes (typical thickness around 500 μm), due to the gauge volume employed ($1 \times 1 \times 10\,mm^3$). Consequently, stress gradients close to the interface between individual tapes cannot be resolved, which explains the flat profiles observed.

No significant differences can be observed between composites with the same composition from conventional slip casting (Fig. 5) and the novel tape casting routes (Fig. 6), according to the stress behavior of Al_2O_3 matrix and Y-TZP particles in composites. This seems to indicate that the low pressure (18 MPa) used for stacking tapes in the novel tape casting green process did not lead to additional macro-residual stresses after sintering. Consequently, the micro-residual stresses in both phases were mainly induced by thermal and elastic mismatch between phases.

However, the mean phase stresses changed as a function of Y-TZP content in composites. Irrespective of the fabrication process (slip casting or tape casting), as Y-TZP content

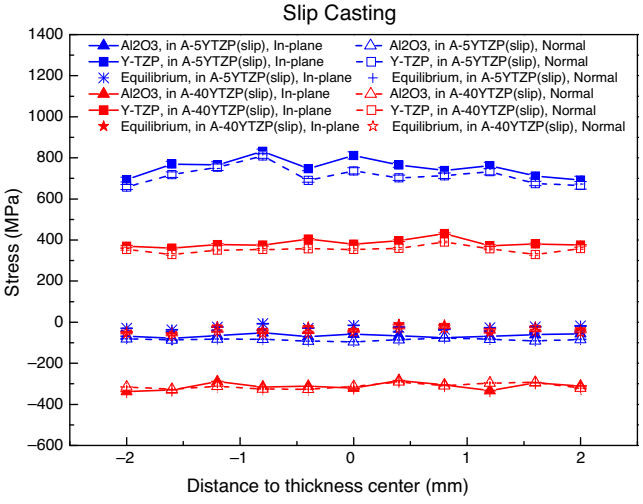

Fig. 5 – Mean phase stress profiles for Al_2O_3 (Δ) and Y-TZP (□) phase along thickness of A/Y-TZP (slip casting) bulk samples, both in the in-plane and normal directions. The values of $f_A\sigma_A + f_{YTZP}\sigma_{YTZP}$ were presented without line.

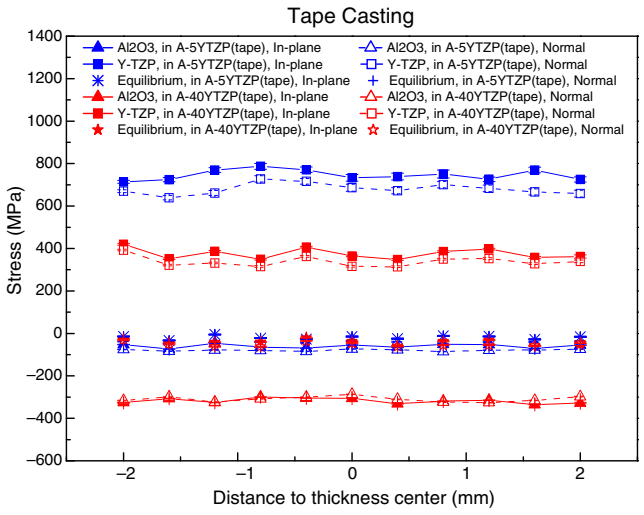

Fig. 6 – Mean phase stress profiles for Al_2O_3 (Δ) and Y-TZP (□) phase through the thickness of A/Y-TZP(tape casting) bulk samples, both in the in-plane and normal directions. The values of $f_A\sigma_A + f_{YTZP}\sigma_{YTZP}$ were presented without line.

increasing from 5 vol.% to 40 vol.%, tensile stresses in Y-TZP particles were decreased from an average value of 750 MPa in A-5YTZP composites to approximately 400 MPa in A-40YTZP composites. On the contrary, the compressive stresses in Al_2O_3 matrix were increased (in absolute value) from an average value of −70 MPa in A-5YTZP composites to approximately −320 MPa in A-40YTZP composites. This behavior agrees with the trends observed in the literature [24]. These values are different from those reported for single reflection scanning by constant-wavelength neutron diffraction [27], where tensile stresses of around 2200 MPa in zirconia and compressive residual stresses of around −200 MPa in alumina were reported for A-5YTZP composites. The difference may be due to the elastic anisotropy associated to the Y-TZP (2 1 1) peak measured in [27]. It is well known that in single peak measurements, the magnitude of the calculated residual stress is highly dependent on the particular reflection used for analysis. On the other hand, the results obtained in this paper are similar to those reported in [16], where residual stresses were determined by piezospectroscopy in the same materials investigated in this work. In [16], the hydrostatic component of the residual stresses in both phases was calculated from experimental measurements in the alumina phase and by imposing the static equilibrium condition (Eq. (10)) in the zirconia phase. The residual stresses reported in [16] for A-5YTZP composites are equal to −50 MPa for the alumina phase, whereas in our case the average value is around −70 MPa. Taking into account that the typical error associated to residual stress measurements is approximately 20 MPa, both results appear quite close. If the static equilibrium condition is applied, in the case of the A-5YTZP (95% alumina, 5% zirconia) this error would translate into approximately 200 MPa when the residual stresses in the zirconia phase are calculated. This would explain the difference between our results in the zirconia phase (750 MPa) and the ones reported in [16] for the A-5YTZP composite in the same phase (950 MPa).

In addition, residual stresses measurements along the in-plane and normal directions were employed to detect possible orientation effects in samples due to the fabrication routes. No significant differences were found between directions for Al_2O_3 matrix, especially in A-40YTZP composites, although slightly higher tensile stresses in in-plane direction than in normal direction were detected in the zirconia phase.

In this case, residual stresses in a particulate-reinforced composite may arise during cooling from the sintering temperature, due to the mismatch of thermal expansion and elastic constants between matrix and particulates [47]. In addition, as explained above, no $t \rightarrow m$ transformation occurred in zirconia during the cooling process, and consequently, residual stresses in A/Y-TZP composites were supposed to have thermal origin.

The modified Eshelby model proposed by Taya et al. [47] was used to estimate the residual stresses in Al_2O_3/Y-TZP composites, in order to confirm the diffraction measurement results. As the densities were close to the theoretical values, composites were assumed to have no voids and consisting of two phases: α-Al_2O_3 matrix with its volume fraction of f_m and Y-TZP reinforcement particulates with volume fraction f_P. The thermal residual strain due to mismatch of thermal expansion coefficients of matrix and particulates, called CTE misfit strain ε^* is given by:

$$\varepsilon^* = \int_{T_P}^{T_{Room}} (\alpha_p - \alpha_m)\delta dT \tag{7}$$

where α_m and α_P are the thermal expansion coefficients of Al_2O_3 matrix and Y-TZP particulates, respectively, δ is the isotropic tensor (Kronecker's delta), T_{Room} are the room temperature and T_P are the effective freezing temperature [48], which was estimated to be 1200 °C in the present Al_2O_3/Y-TZP system [49]. As highly dense composites, the isotropic average stress fields in the particulate, σ_p, and in the matrix, σ_m, can be estimated as [47]:

$$\frac{\sigma_p}{E_m} = \frac{-2f_m\beta\varepsilon^*}{A} \tag{8}$$

$$\frac{\sigma_m}{E_m} = \frac{2f_P\beta\varepsilon^*}{A} \tag{9}$$

where $A = f_m(\beta+2)(1+\nu_m) + 3\beta f_p(1-\nu_m)$, $\beta = \frac{(1+\nu_m)}{(1-2\nu_p)}\left(\frac{E_p}{E_m}\right)$, ε^* is the CTE misfit strain, f_i, E_i and ν_i are the volume fraction, elastic modulus and Poisson's ratio of i phase, where $i = m$ and P represent Al_2O_3 matrix and Y-TZP particulates, respectively.

Based on Eq. (7), with $\alpha_p > \alpha_m$ in A/Y-TZP composites, CTE misfit strain would be negative during cooling from the freezing temperature to room temperature. Consequently, tension in Y-TZP particulates and compression in Al_2O_3 matrix were expected, in good agreement with the experimental results by neutron diffraction. Irrespective of different processing techniques and grain size effect, the average thermal residual stresses in Y-TZP phase and Al_2O_3 phase in A-5YTZP and

A-40YTZP composites can be estimated according to Eqs. (8) and (9):

In A-5YTZP composites: $\sigma^{\text{Y-TZP}}_{\text{A-5YTZP}} = 741$ MPa, $\sigma^{\text{A}}_{\text{A-5YTZP}} = -39$ MPa;
In A-40YTZP composites: $\sigma^{\text{Y-TZP}}_{\text{A-40YTZP}} = 489$ MPa, $\sigma^{\text{A}}_{\text{A-40YTZP}} = -326$ MPa.

A decrease of the tensile stress in Y-TZP phase and an increase of the absolute value of compressive stress in Al_2O_3 matrix with the volume fraction of Y-TZP is found, which agrees very well with the ND experimental results.

The microstructure development should also be taken into account. As described in Fig. 3 and Table 1, with more zirconia content, the grain size of Al_2O_3 matrix was reduced but the one of Y-TZP was slightly increased. For a single Y-TZP particle, its connectivity with the Al_2O_3 matrix would be decreased but the one between Y-TZP particulates would be enhanced. The internal tensile stresses on Y-TZP particulates, which were caused by the thermal and elastic mismatch with the surroundings, were correspondingly weakened. In contrast, the increase of Y-TZP particles would cause a separation in the Al_2O_3 matrix, resulting in more contact areas between Al_2O_3 matrix and Y-TZP particles; consequently, compressive stress on Al_2O_3 matrix was increased.

The calculated residual stresses in the alumina matrix by using the modified Eshelby model proposed by Taya [47] were very similar to those obtained by neutron diffraction measurements in this work, especially in A-40YTZP composites. Such a good agreement was also observed for the residual stresses in the zirconia phase in A-5YTZP composites. As Y-TZP content increased to 40 vol.%, the tensile residual stress in the zirconia phase obtained from neutron diffraction measurements was slightly lower than the model predictions. According to recent work by C. Exare et al. [50], the attrition on alumina and zirconia slurries by high energy milling will influence the stability of the different zirconia phases and generate compressive residual stresses. Although in the present work ball milling was used, the possibility that compressive residual stresses might be generated in zirconia should not be completely ruled out, especially when the volume fraction of zirconia is increased. This in turn might help to explain the differences observed between the residual stresses measured in zirconia by neutron diffraction and the model predictions.

It was initially assumed the macro-residual stresses as negligible in all A/Y-TZP bulk samples since no pressure was applied during sintering process. The equilibrium of mean phase residual stresses of Y-TZP particles and Al_2O_3 matrix was checked by using the static equilibrium condition for residual stresses [51]:

$$f_A\sigma_A + f_{YTZP}\sigma_{YTZP} = 0 \quad (10)$$

where f_A, f_{YTZP} are the volume fractions of Al_2O_3 matrix and Y-TZP in composites; and σ_A, σ_{YTZP} are the measured mean phase stress of Al_2O_3 matrix and Y-TZP particulates, respectively. The values of Eq. (10) through thickness were plotted in Figs. 5 and 6 for tape and slip casting samples. It can be seen that in all cases the static equilibrium condition is approximately verified.

Summary and conclusions

Based on the analysis of microstructure and the internal residual stresses in Al_2O_3/Y-TZP bulk composites fabricated by different green processing techniques (a novel tape casting and conventional slip casting) and with different Y-TZP content, the following main results and conclusions were presented:

(1) The tetragonal to monoclinic transformation of zirconia was controlled in the studied A/Y-TZP composites during sintering process, leading to almost full retention of tetragonal zirconia phase in composites after fabrication, as shown by Rietveld profile analysis.
(2) Grain size and microstructure of materials changed with the Y-TZP volume fraction in composites. The grain size of Al_2O_3 matrix was reduced and the grain size of Y-TZP was slightly increased when the volume fraction Y-TZP was increased.
(3) Due to mismatch in thermal expansion between matrix and particles, tensile residual stresses developed in Y-TZP particulates and compressive ones in Al_2O_3 matrix. Almost flat through-thickness residual stress profiles were obtained in both phases. With increasing Y-TZP content in composites, a decrease in tensile stress in Y-TZP phase and an increase in compressive stress (absolute values) in Al_2O_3 matrix was found. No obvious orientation effects were discovered, according to the similar results in normal and in-plane directions. Residual stresses for both phases were mainly dependent on the Y-TZP content in composites; irrespective of sample orientation (in-plane and normal directions) and fabrication processes (slip casting and tape casting). The residual stress values obtained from neutron diffraction measurements are consistent with those reported in the literature as well as with the predictions of a modified Eshelby model.
(4) No obvious effects were induced by the different fabrication processes (the novel tape casting and conventional slip casting), in terms of residual stresses, densities and grain sizes in the studied A/Y-TZP ceramics.

Acknowledgments

This research has been supported by the Spanish Ministry of Science and Innovation through grants BIA2011-26486 and BIA2014-53314-R. EU-NIM3 funding under the program 'Access to ISIS Neutrons' is acknowledged for the measurements at ISIS ENGIN-X. One of the authors (Kunyang Fan) would like to thank China Scholarship Council (CSC) for the grant (No. 2011637148) to do a Ph.D. in Spain.

REFERENCES

[1] B. Basu, J. Vleugels, O. Van Der Biest, ZrO_2–Al_2O_3 composites with tailored toughness, J. Alloys Compd. 372 (2004) 278–284.
[2] V. Naglieri, P. Palmero, L. Montanaro, J. Chevalier, Elaboration of alumina–zirconia composites: role of the zirconia content

on the microstructure and mechanical properties, Materials 6 (2013) 2090–2102.
[3] K. Kageyama, Y. Harada, H. Kato, Preparation and mechanical properties of alumina–zirconia composites with agglomerated structures using pre-sintered powder, Mater. Trans. 44 (2003) 1571–1576.
[4] F. Gutierrez-Mora, D. Singh, N. Chen, K.C. Goretta, J.L. Routbort, S.H. Majumdar, A. Dominguez-Rodriguez, Fracture of composite alumina/yttria-stabilized zirconia joints, J. Eur. Ceram. Soc. 26 (2006) 961–965.
[5] W. Tuan, R. Chen, T. Wang, C. Cheng, P. Kuo, Mechanical properties of Al_2O_3/ZrO_2 composites, J. Eur. Ceram. Soc. 22 (2002) 2827–2833.
[6] A. Nevarez-Rascon, A. Aguilar-Elguezabal, E. Orrantia, M.H. Bocanegra-Bernal, On the wide range of mechanical properties of ZTA and ATZ based dental ceramic composites by varying the Al_2O_3 and ZrO_2 content, Int. J. Refract. Met. Hard Mater. 27 (2009) 962–970.
[7] R.H. Hannink, P.M. Kelly, B.C. Muddle, Transformation toughening in zirconia-containing ceramics, J. Am. Ceram. Soc. (2000) 461–487.
[8] B. Basu, Toughening of yttria-stabilised tetragonal zirconia ceramics, Int. Mater. Rev. 50 (2005) 239–256.
[9] A.G. Evans, Perspective on the development of high-toughness ceramics, J. Am. Ceram. Soc. 73 (1990) 187–206.
[10] J. Wang, R. Stevens, Zirconia-toughened alumina (ZTA) ceramics, J. Mater. Sci. 24 (1989) 3421–3440.
[11] M. Ruehle, N. Claussen, A.H. Heuer, Transformation and microcrack toughening as complementary processes in ZrO_2-toughened Al_2O_3, J. Am. Ceram. Soc. 69 (1986) 195–197.
[12] Y.S. Shin, Y.W. Rhee, S.J.L. Kang, Experimental evaluation of toughening mechanisms in alumina–zirconia composites, J. Am. Ceram. Soc. 82 (1999) 1229–1232.
[13] N. Claussen, Transformation toughening of ceramics, in: Fracture of Non-Metallic Materials, Springer, 1987, pp. 137–156.
[14] K.B. Alexander, P.F. Becher, X.L. Wang, C.H. Hsueh, Internal stresses and the martensite start temperature in alumina–zirconia composites: effects of composition and microstructure, J. Am. Ceram. Soc. 78 (1995) 291–296.
[15] J.R. Kelly, I. Denry, Stabilized zirconia as a structural ceramic: an overview, Dent. Mater. 24 (2008) 289–298.
[16] C. Baudín, J. Gurauskis, A.J. Sánchez-Herencia, V.M. Orera, Indentation damage and residual stress field in alumina-Y_2O_3-stabilized zirconia composites, J. Am. Ceram. Soc. 92 (2009) 152–160.
[17] M. Guazzato, M. Albakry, S.P. Ringer, M.V. Swain, Strength, fracture toughness and microstructure of a selection of all-ceramic materials. Part II. Zirconia-based dental ceramics, Dent. Mater. 20 (2004) 449–456.
[18] D.J. Green, Critical microstructures for microcracking in Al_2O_3–ZrO_2 composites, J. Am. Ceram. Soc. 65 (1982) 610–614.
[19] G. De Portu, L. Micele, Y. Sekiguchi, G. Pezzotti, Measurement of residual stress distributions in Al_2O_3/3Y-TZP multilayered composites by fluorescence and Raman microprobe piezo-spectroscopy, Acta Mater. 53 (2005) 1511–1520.
[20] P. Parente, Y. Ortega, B. Savoini, M.A. Monge, A. Tucci, L. Esposito, B. Ferrari, A.J. Sanchez-Herencia, Characterization of residual compressive stresses in layered ceramics by positron annihilation spectroscopy, J. Eur. Ceram. Soc. 32 (2012) 3989–3993.
[21] G. de Portu, L. Micele, S. Guicciardi, S. Fujimura, G. Pezzotti, Y. Sekiguchi, Effect of residual stresses on the fracture behaviour of notched laminated composites loaded in flexural geometry, Compos. Sci. Technol. 65 (2005) 1501–1506.
[22] R. Bermejo, Y. Torres, A. Sanchezherencia, C. Baudin, M. Anglada, L. Llanes, Residual stresses, strength and toughness of laminates with different layer thickness ratios, Acta Mater. 54 (2006) 4745–4757.
[23] G. Magnani, A. Brillante, Effect of the composition and sintering process on mechanical properties and residual stresses in zirconia–alumina composites, J. Eur. Ceram. Soc. 25 (2005) 3383–3392.
[24] X.L. Wang, C.R. Hubbard, K.B. Alexander, P.F. Becher, J.A. Fernandez-Baca, S. Spooner, Neutron diffraction measurements of the residual stresses in Al_2O_3–ZrO_2 (CeO_2) ceramic composites, J. Am. Ceram. Soc. 77 (1994) 1569–1575.
[25] J.F. Bartolomé, G. Bruno, A.H. DeAza, Neutron diffraction residual stress analysis of zirconia toughened alumina (ZTA) composites, J. Eur. Ceram. Soc. 28 (2008) 1809–1814.
[26] T. Adachi, T. Sekino, T. Nakayama, T. Kusunose, K. Niihara, Measurement of microscopic stress distribution of multilayered composite by X-ray stress analysis, Mater. Lett. 57 (2003) 3057–3062.
[27] J. Ruiz-Hervías, G. Bruno, J. Gurauskis, A.J. Sánchez-Herencia, C. Baudín, Neutron diffraction investigation for possible anisotropy within monolithic Al_2O_3/Y-TZP composites fabricated by stacking together cast tapes, Scr. Mater. 54 (2006) 1133–1137.
[28] J. Ruiz-Hervias, G. Bruno, J. Gurauskis, A.J. Sanchez-Herencia, C. Baudin, Residual stresses in Al_2O_3/Y-TZP ceramic laminates fabricated by tape and slip casting, Mater. Sci. Forum 571–572 (2008) 327–332.
[29] G.A. Webster, R.C. Wimpory, Non-destructive measurement of residual stress by neutron diffraction, J. Mater. Process. Technol. 117 (2001) 395–399.
[30] P.J. Withers, Mapping residual and internal stress in materials by neutron diffraction, Comptes Rendus Phys. 8 (2007) 806–820.
[31] H. Rietveld, A profile refinement method for nuclear and magnetic structures, J. Appl. Crystallogr. 2 (1969) 65–71.
[32] A. Tsetsekou, C. Agrafiotis, A. Milias, Optimization of the rheological properties of alumina slurries for ceramic processing applications Part I: Slip-casting, J. Eur. Ceram. Soc. 21 (2001) 363–373.
[33] J. Gurauskis, A. Sanchez-Herencia, C. Baudin, Joining green ceramic tapes made from water-based slurries by applying low pressures at ambient temperature, J. Eur. Ceram. Soc. 25 (2005) 3403–3411.
[34] J. Gurauskis, A.J. Sánchez-Herencia, C. Baudín, Al_2O_3/Y-TZP and Y-TZP materials fabricated by stacking layers obtained by aqueous tape casting, J. Eur. Ceram. Soc. 26 (2006) 1489–1496.
[35] J. Santisteban, M. Daymond, J. James, L. Edwards, ENGIN-X: a third-generation neutron strain scanner, J. Appl. Crystallogr. 39 (2006) 812–825.
[36] A. Coelho, TOPAS-Academic V5, Coelho Software, Brisbane, Australia, 2012, http://www.topas-academic.net/.
[37] A.C. Larson, R.B. Von Dreele, GSAS, General Structure Analysis System, LANSCE, MS-H805, Los Alamos, New Mexico, 1994.
[38] C. Howard, R. Hill, B. Reichert, Structures of ZrO_2 polymorphs at room temperature by high-resolution neutron powder diffraction, Acta Crystallogr. Sect. B: Struct. Sci. 44 (1988) 116–120.
[39] M. Yashima, S. Sasaki, M. Kakihana, Y. Yamaguchi, H. Arashi, M. Yoshimura, Oxygen-induced structural change of the tetragonal phase around the tetragonal–cubic phase boundary in ZrO_2–YO1.5 solid solutions, Acta Crystallogr. Sect. B: Struct. Sci. 50 (1994) 663–672.
[40] J. Lewis, D. Schwarzenbach, H. Flack, Electric field gradients and charge density in corundum, α-Al_2O_3, Acta Crystallogr. Sect. A: Cryst. Phys. Diffr. Theor. Gen. Crystallogr. 38 (1982) 733–739.

[41] L. McCusker, R. Von Dreele, D. Cox, D. Louer, P. Scardi, Rietveld refinement guidelines, J. Appl. Crystallogr. 32 (1999) 36–50.
[42] M. Daymond, M. Bourke, R. Von Dreele, B. Clausen, T. Lorentzen, Use of Rietveld refinement for elastic macrostrain determination and for evaluation of plastic strain history from diffraction spectra, J. Appl. Phys. 82 (1997) 1554–1562.
[43] H. Choo, M. Bourke, P. Nash, M. Daymond, N. Shi, Thermal residual stresses in NiAl–AlN–Al_2O_3 composites measured by neutron diffraction, Mater. Sci. Eng. A 264 (1999) 108–121.
[44] W. Pabst, G. Ticha, E. Gregorova, Effective elastic properties of alumina–zirconia composite ceramics-Part 3. Calculation of elastic moduli of polycrystalline alumina and zirconia from monocrystal data, Ceramics-Silikaty 48 (2004) 41–48.
[45] B. Basu, J. Vleugels, O.V.D. Biest, Transformation behaviour of tetragonal zirconia: role of dopant content and distribution, Mater. Sci. Eng. A 366 (2004) 338–347.
[46] S. Deville, J. Chevalier, G. Fantozzi, J.F. Bartolomé, J.n. Requena, J.S. Moya, R. Torrecillas, L.A. Dıáz, Low-temperature ageing of zirconia-toughened alumina ceramics and its implication in biomedical implants, J. Eur. Ceram. Soc. 23 (2003) 2975–2982.
[47] M. Taya, S. Hayashi, A.S. Kobayashi, H. Yoon, Toughening of a particulate-reinforced ceramic–matrix composite by thermal residual stress, J. Am. Ceram. Soc. 73 (1990) 1382–1391.
[48] J. Blendell, R.L. Coble, Measurement of stress due to thermal expansion anisotropy in Al_2O_3, J. Am. Ceram. Soc. 65 (1982) 174–178.
[49] J. Ramírez-Rico, J. Martínez-Fernández, J. Peña, D. Singh, J. Routbort, Residual stresses in Al_2O_3–ZrO_2 (3 mol.% Y_2O_3) directionally solidified eutectic ceramics as a function of temperature, Mater. Sci. Eng. A 541 (2012) 61–66.
[50] C. Exare, J.-M. Kiat, N. Guiblin, F. Porcher, V. Petricek, Structural evolution of ZTA composites during synthesis and processing, J. Eur. Ceram. Soc. 35 (2015) 1273–1283.
[51] V. Hauk, Structural and Residual Stress Analysis by Nondestructive Methods: Evaluation-Application-Assessment, Elsevier, 1997.